ACCESSIBILITY

OsloMet – Oslo Metropolitan University

Department of Civil Engineering & Energy Technology
Section of Civil Engineering

Master Program in Structural Engineering & Building Technology

MASTER THESIS

TITLE OF REPORT	DATE
Tensile resistance of bolts in threaded holes	24.05.2023
	PAGES / ATTACHMENTS 48/
AUTHOR(S) Viktoriia Eriksen	SUPERVISOR(S) Aase Reyes Erik Grimsmo

IN COLLABORATION WITH	CONTACT PERSON

SUMMARY / SYNOPSIS

There are many standards governing bolted connections. Bolts in threaded holes are not however fully covered by them. Current Eurocodes determine only minimum thickness of steel plates, but length and width are not governed. The current thesis will investigate several bolt and plate assemblies of various sizes to ascertain how plate shape affects threaded assembly performance. To simulate the behavior of threaded connections subjected to tensile load, bolt and plate assemblies will be modelled using Abaqus FEM Software.

KEYWORDS
Threaded connections
Tensile tests
FEM

Preface

I would like to thank my superiors, Professor Aase Reyes, and Associate Professor Erik Grimsmo, for their guidance and help. Their assistance was essential to the development of the thesis. A special thanks to Erik Grimsmo for his prompt answer and patience.

I would also like to thank Professor Vagelis Plevris and Stipendiat Sigbjørn Tveit for the assistance with the employment of Abaqus FEM Software.

Viktoriia Eriksen

Contents

List of Figures

1. Introduction

Today bolts are popular components in machine and building design. From the small screws in door hinges to the large bolts in skyscrapers, they hold everything together. The history of the bolts can be divided into two parts: the threads, which date back to 400 BC and were used for things like a spiral for lifting water and presses for grapes to make wine, and the fasteners themselves, which have been in use for about 400 years. Most researchers agree that the Industrial Revolution accelerated the development of the contemporary nut and bolt. The inconsistency of screw threads in various nations caused a significant barrier to the war effort during World War I, and it worsened for the Allies throughout World War II. The Unified thread was adopted as the standard in 1948 by the UK, the USA, and Canada and all nations that utilized imperial measurements. This resulted in the development of the ISO metric thread, which is now utilized in almost all nations. (Nord-Lock, 2023)

Currently, there are many standards governing bolted connections. However, bolts in threaded (tapped) holes have no design specifications in Eurocode. There will be guidelines for this subject in the updated edition of EN 1993-1-8 (CEN, 2023). According to the coming regulations, steel plates must have a minimum thickness in order to fully utilize tensile resistance of the bolts in tension. Yet, the regulations do not govern length and width of the connecting plates. A large plate may distort significantly when a bolt is under tension. It can potentially affect the thread connection between the plate and bolt and moreover decrease the tensile resistance of the bolted connection as a result.

1.1. Scope of thesis

The objective of the present thesis is to study different assemblies of bolt and plates of various sizes to investigate how geometry of the plate affects performance of threaded assemblies.

For this purpose, relevant literature was studied. Subsequently finite element model with accordance to the governing standards was developed. In order to reduce a computational cost, axisymmetric model was chosen. Material data used in the present thesis was provided by earlier studies made by E. Grimsmo, E. Skavhaug and S. Østhus.

2. Literature review

For the better understanding of the research topic, a study of the relevant literature was performed. The aim was to learn about previous tests of bolted connections as well as the theoretical basis. A summary of some publications is presented in this chapter.

Grimsmo (2017) investigated effect of the nut placement on a failure of bolt-and-nut assembly. Authors performed tensile tests on various M16 bolt-and-nut assemblies (Fig. 1). The results of experimental tests (see Fig. 2) showed that thread failure occurred in assemblies where the nut was placed near the shank, the unthreaded part of the bolt. When the nut was sufficiently distant from the thread run-out, assemblies were damaged by bolt fracture. Numerical simulations of the experimental tests revealed that if the nut is placed too close to the thread run-out, the bolt will neck. This can cause a thread failure in testing as well as in simulations.

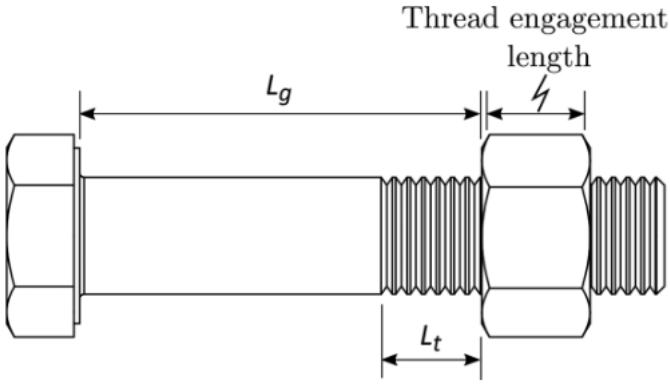

Figure 1 Illustration of grip length L_g, threaded length L_t, and threaded engagement length (Grimsmo et al., 2017)

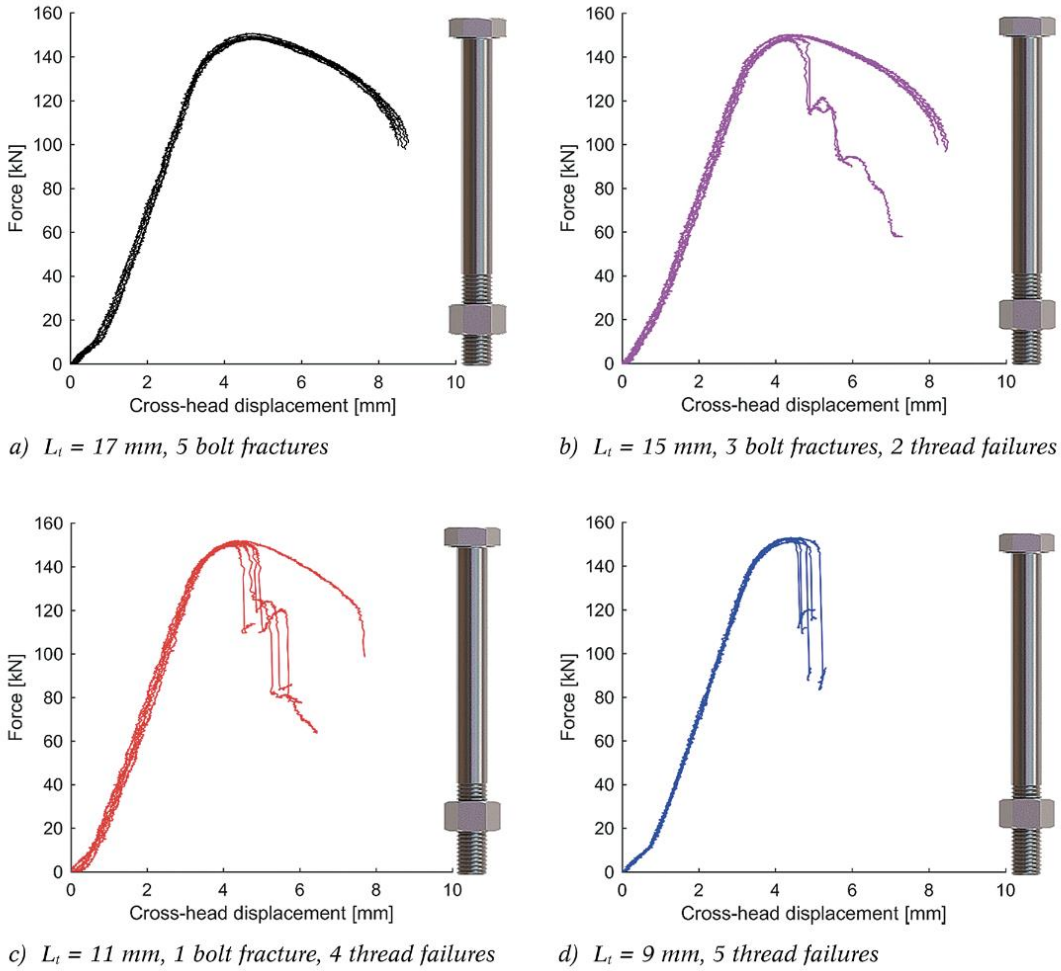

Figure 2 Test-derived force-displacement curves. Every threaded length was subjected to five replicate tests. (Grimsmo et al., 2017)

M. J. O'Brien and R. G. Metcalfe (2009) in their article examined the design elements of fasteners. Their goal was to address the issue of fatigue resistance failure. It was found that stress concentrations like a notch can significantly reduce a component's lifespan since they increase locally applied stress. Thus, a V-notch would be the worst option in terms of stress concentrations and fatigue susceptibility. The stress field however can be altered by a succession of neighboring notches, as shown in Fig. 3, as opposed to a single V-notch, which can represent a severe concentration of stresses.

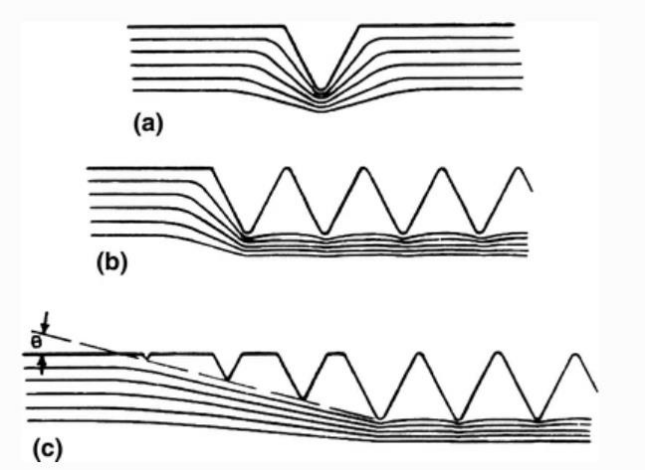

Figure 3 The numerous threads' impact on the stress field (O'Brien & Metcalfe, 2009)

The stress concentration especially poses a significant threat in the area connected to the fastener and nut's initial thread. Because the initial thread tends to carry the largest load of all the engaged threads and has only one adjacent load-carrying thread, the stress concentration in the thread root is highest at this thread (see Fig. 4). Design and production techniques may be used to lessen the consequences of stress concentration. Moreover, the stress concentration at the first few threads will be reduced by providing at least two full fastener threads (up to one diameter) above and below the nut.

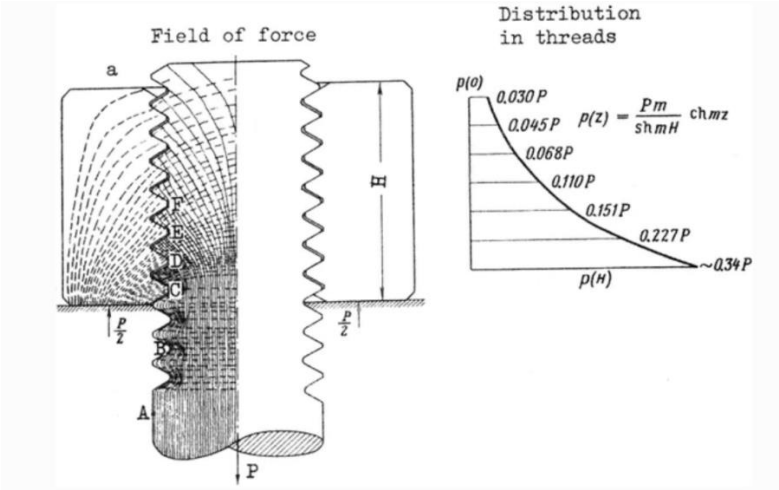

Figure 4 Principal stresses and the field of force in a nut-fastener (O'Brien & Metcalfe, 2009)

Alexander (1977) studied possible failure modes of fastener assembly. He concluded that internal thread stripping is one of the most common reasons for failure of fasteners exposed to static tensile overload. The threads of the nuts and bolts are elastically distorted under applied loads, and in the case of sufficiently large loads, plastically deformed or bent. This thread bending reduces the effective shear area and presents a contact surface at a smaller angle to the bolt axis. It generates a stronger mechanical advantage for the wedging action of the threads and subsequently for nut dilatation. Figure 5 depicts the resulting loss of strength. Curve C3 declines and then flattens out when strength ratio R_s approaches unity when it rises from the extreme low values. The cause of this effect is that the bolt thread has a significant strength surplus and does not flex significantly for low values of R_s. When R_s rises, the strength difference between the bolt and nut threads is lessened, allowing for more thread bending, which reduces the effective shear area and causes the nut to dilate more.

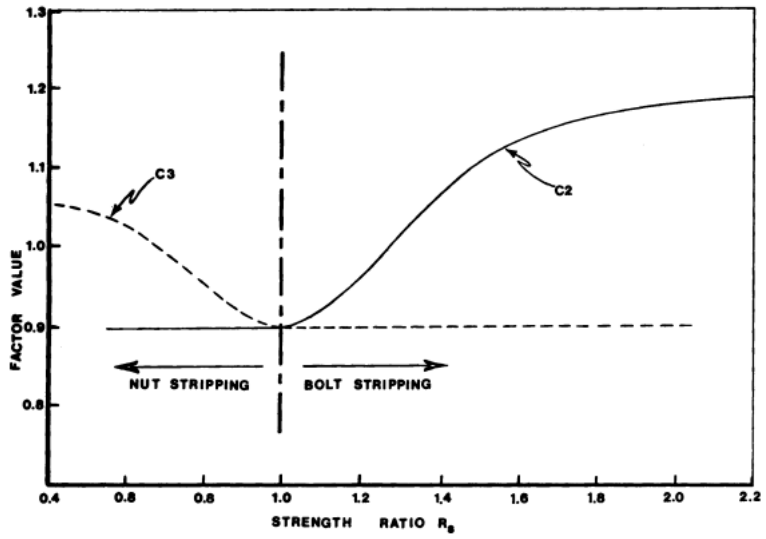

Figure 5 Thread bending strength reducing factors (Alexander, 1977)

3. Material mechanics

Accurate material modelling is important when the finite element models are built to conduct stress analysis. The reason for this is that different materials may behave differently even when subjected to the same geometry, loads, and boundary conditions.

Another important aspect is a correct stress-strain curve obtained by tensile tests. Typical stress-strain curve consists of elastic and plastic parts. As seen in Fig. 6 the strain vector can be decomposed into elastic and plastic segments:

$$\varepsilon = \varepsilon^e + \varepsilon^p \tag{3.1}$$

This chapter will present both elastic and plastic aspects of material.

3.1. Elasticity

Elasticity is the first domain in the stress-strain curve. Where stress (engineering stress) σ is equal to the applied force divided by the area that is not distorted by the force being applied. Strain, ε is a measure of deformation and is defined as the change in length divided by the original length. Stretching of atomic bonds results in elastic deformation. This stretching is totally reversible when the stress is released, unlike the dislocation motion

The majority of metals are isotropic materials. It means that they have same properties in all directions. Hence, there are two parameters that affect elastic domain of metals: Young's Modulus and Poisson's ratio. The modulus of elasticity, or Young's modulus, E is the slope of the straight line forming the elastic zone in the stress-strain diagram. Young's modulus measures the stiffness of a substance. It is used to determine how much a part will bend or stretch when a load is applied, but only up to the elastic limit. The Young's modulus is the ratio between stress, σ and strain, ε.

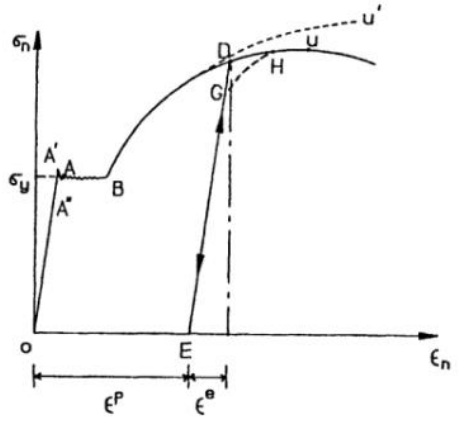

Figure 6 Stress-strain curve under uniaxial loading (Huang, 1995)

According to Hooke's law, elastic bodies can only fully restore their former structure up to an elastic limit. Within the elastic limit, the materials extension is directly proportional to the applied load. This implies that inside the elasticity domain, stress and strain are directly proportional:

Hooke's law:

$$\sigma = E\varepsilon \tag{3.2}$$

Poisson's ratio, ν is a dimensionless property that demonstrates how much a specific material will contract laterally in response to longitudinal pulling force. Poisson's ratio, ν is described as a ratio between negative lateral strain, $-\varepsilon_{lateral}$ and longitudinal strain, $\varepsilon_{longitudinal}$.

$$\nu = \frac{-\varepsilon_{lateral}}{\varepsilon_{longitudinal}} \tag{3.3}$$

3.2. Plasticity

Loading material beyond its yield stress point (lower yield point is indicated as A in Fig. 6) leads to plastic deformation. In the elastic domain the loading and unloading curves follow the same paths, but in the plastic domain the loading and unloading paths are different. In this chapter three main parts in the plasticity theory: yield criteria, flow rule and hardening law will be described.

3.2.1. Yield Criteria

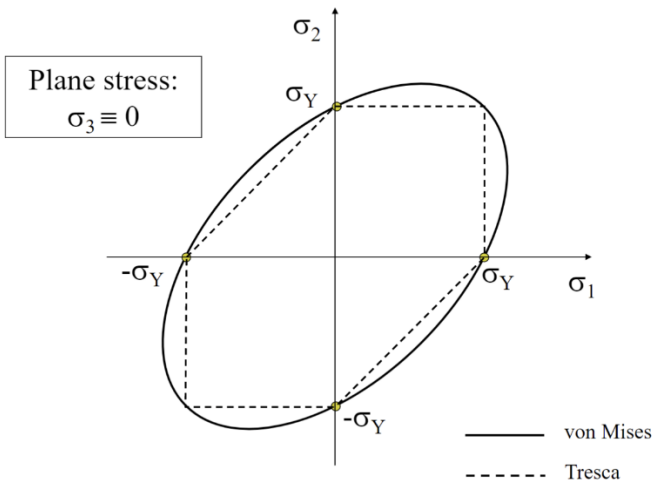

Figure 7 Tresca and Von Mises yield criterion (Reyes, 2022)

Yield point is the point of the initiation of plastic deformation. Yield criteria describes the failing behaviour of the material under load. There are two important yield criteria: Tresca criterion and Von Mises criterion (Fig.7).

Tresca criterion is also called maximum stress theory. According to the yield criterion, yielding happens when the highest shear stress equals the shear stress at yielding in a uniaxial tension test. Assuming that principal stresses are:

$$\sigma_{max} = \sigma_1 \tag{3.4}$$

$$\sigma_{min} = \sigma_3 \tag{3.5}$$

Maximum stress theory can be expressed as:

$$\sigma_1 - \sigma_3 = \sigma_y \tag{3.6}$$

Von Mises criterion is also called maximum distortion energy theory. According to Von Mises, when the distortional strain energy density reaches the value at yielding in uniaxial tension, yielding in a multi-axial stress condition occurs. For general stress state Von Mises criterion is defined by:

$$(\sigma_1 - \sigma_2)^2 + (\sigma_2 - \sigma_3)^2 + (\sigma_3 - \sigma_1)^2 = 2{\sigma_Y}^2 \tag{3.7}$$

In plane stress states, assuming that $\sigma_z = \tau_{zx} = \tau_{yz} = 0$, Von Mises criterion is:

$${\sigma_x}^2 + {\sigma_y}^2 - \sigma_x\sigma_y + 3{\tau_{xy}}^2 = {\sigma_Y}^2 \tag{3.8}$$

Alternative interpretation of Von Mises theory states that when effective stress becomes equal to the yield stress in uniaxial direction, i.e. $\sigma_e = \sigma_Y$, Von Mises criterion can be expressed as:

$$\sigma_e = \frac{1}{\sqrt{2}} [\,(\sigma_1 - \sigma_2)^2 + (\sigma_2 - \sigma_3)^2 + (\sigma_3 - \sigma_1)^2]^{\frac{1}{2}} \tag{3.9}$$

3.2.2. Plastic Flow rule

The material flow beyond initial yield is mathematically described by the flow rule. The relationship between plastic strain and stress is a straightforward way to represent it, as in the elastic domain this relation is represented by Hooke's law. Plastic deformations are irreversible and path dependent. Hence, formulation in flow rule is incremental.

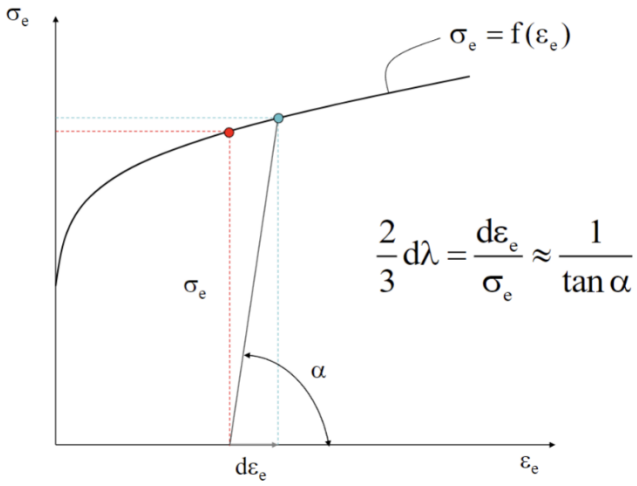

Figure 8 Graphic representation of graphic multiplier dλ (Reyes, 2022)

Levi-Mises equation implies that material is isotropic and the elastic strains are negligible:

$$\frac{d\varepsilon_1}{s_1} = \frac{d\varepsilon_2}{s_2} = \frac{d\varepsilon_3}{s_3} = d\lambda \tag{3.10}$$

where $d\lambda$ is plastic multiplier (Fig.8).

Combining the von Mises effective stress expression and the Levy-Mises flow rule:

$$\frac{d\varepsilon_e}{\sigma_e} = \frac{2}{3} d\lambda \tag{3.10}$$

For plastic deformation processes, incremental plastic work should be larger than or equal to zero: $\varsigma' d\varepsilon^p \geq 0$.

Effective plastic strain increment:

$$d\varepsilon_e = \left[\frac{2}{3}\left(d\varepsilon_1{}^2 + d\varepsilon_2{}^2 + d\varepsilon_3{}^2\right)\right]^{\frac{1}{2}} = d\varepsilon_1 \tag{3.11}$$

The Levi- Mises flow rule can be expressed:

$$d\varepsilon_1 = d\lambda' \frac{\delta f}{\delta \sigma_1} \tag{3.11}$$

$$d\varepsilon_2 = d\lambda' \frac{\delta f}{\delta \sigma_2} \tag{3.12}$$

$$d\varepsilon_3 = d\lambda' \frac{\delta f}{\delta \sigma_3} \tag{3.13}$$

3.2.3. Work hardening rule

Hardening rules explain how the yield surface or locus changes as a result of plastic deformation brought on by the material's work hardening.

Perfectly plastic behaviour is indicated as segment AB in Fig.6. If material stress keeps increasing after it reaches point B, material starts to harden. Hardening will continue up until it reaches point U, also known as ultimate stress. Segment BU is a work hardening region (Huang, 1995).

Isotropic hardening rule can be written as:

$$\sigma_y = \sigma_0 + R(\varepsilon_e) \tag{3.14}$$

According to the Voce rule (Fig. 9), the hardening variable can be expressed:

$$R(\varepsilon_e) = Q(1 - \exp(-C\varepsilon_e) \tag{3.15}$$

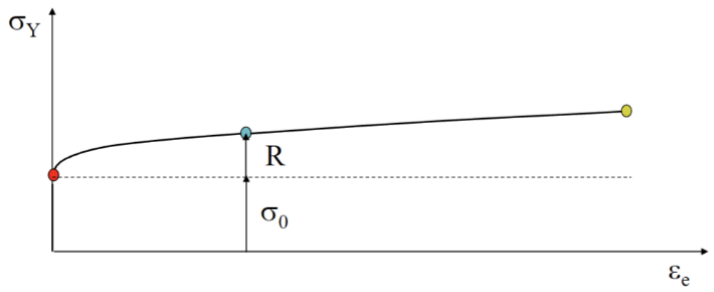

Figure 9 Voce Rule hardening illustration (Reyes, 2022)

3.3. Identification of material parameters

Material properties are usually characterized by uniaxial tension test results. In order to retrieve material properties up to necking, the engineering stress and strain are extracted from the test and converted to real stress and strain.

Engineering stress σ is calculated by dividing the applied load, F by the material's initial cross-sectional area A_0. It is referred to as nominal stress.

$$\sigma = \frac{F}{A_0} \tag{3.15}$$

Engineering strain ε is the ratio of the amount of deformation in the direction of the applied force $(L - L_0)$ to the material's initial length L_0. It is referred to as a nominal strain.

$$\varepsilon = \frac{L - L_0}{L_0} \tag{3.16}$$

Engineering stress and strain differ from true stress and strain. True stress in a tensile test exceeds engineering stress, but true strain falls short of engineering strain. With plastic deformation, the gap between the actual stresses and strains and engineered stresses and strains will widen. The differences between the two are insignificant for low strains in the elastic range.

True stress σ_t is the amount of tension produced when an instantaneous load F is applied to a cross-sectional region A.

$$\sigma_t = \frac{F}{A} \tag{3.17}$$

Engineering strain is linear, whereas true strain ε_t is logarithmic.

$$\varepsilon_t = \int \frac{\delta L}{L} \tag{3.18}$$

The displacement/deformation of a structural member subjected to external loading is measured by using the non-contact, non-interferometric optical technique known as digital image correlation (DIC). The DIC method's concept is based on the ideas of continuum mechanics. A digital camera and specialized computer software make up the majority of the system. Before and after the deformation phase, a camera is used to take a series of photographs of the surface of the tested object. The DIC program analyses the acquired digital image data (a set of images) using mathematical correlation. A set of displacement/deformation maps are then produced for the complete specimen surface. From strain fields, stress fields can be assessed.

Hardness value of the material is obtained by the Vickers hardness test method, also known as a microhardness test method. It is based on an optical measurement instrument where the Microhardness test process specifies a range of light stresses utilizing a diamond indenter to create an imprint that is measured and converted to a hardness parameter.

3.3.1. Calibration of material parameters

Uniform stress-strain relation is only valid until necking. After necking, the stress state shifts from uniaxial stress to triaxial stress. It is possible to calibrate the material properties by using Bridgman's corrective procedure. The Bridgman's approach necessitates the continuous measurement of the diameter of the neck's narrowest cross-section and the radius of curvature of the neck's axisymmetric neck profile in the axial loading direction (Wang & Tong, 2015). The mean true axial strain and the mean true axial stress are determined by a given post-peak axial load P and the current area of the narrowest cross-section of the neck A.

$$\bar{\varepsilon}_{ave} = \ln(\frac{A_0}{A}) \tag{3.19}$$

$$\bar{\varsigma}_{ave} = \frac{P}{A} = \frac{P}{A_0} e^{\bar{\varepsilon}_{ave}} \tag{3.19}$$

where A_0 is the initial area of the circular cross-section of the gage section of a cylindrical tension sample.

After the triaxial stress's component is eliminated by Bridgman's procedure, Voce rule isotropic hardening is applied. The fundamental tenet of elastic-plastic constitutive relationships is the presumption that some materials can withstand minor elastic (recoverable) as well as plastic (permanent) strains at each loading increment. Furthermore, it is expected that elastic-viscoplastic materials exhibit rate-dependent behavior in the plastic zone.

$$\sigma_{eq} = \begin{cases} \sigma_y, & \varepsilon_p < \varepsilon_{p,plat} \\ \left[\sigma_y + \sum_{i=1}^{2} Q_i \left(1 - exp\left(-\frac{\theta_i}{Q_i}\left(\varepsilon_p - \varepsilon_{p,plat}\right)\right)\right)\right] \left[1 + \frac{\dot{\varepsilon}_p}{\dot{\varepsilon}_{ref}}\right]^{-C}, & \varepsilon_p \geq \varepsilon_{p,plat} \end{cases} \quad (3.20)$$

where:

σ_y	Yield stress
Q_i, θ_i	hardening constants of the extended hardening rule
ε_p	equivalent plastic strain
$\varepsilon_{p,plat}$	value of ε_p at the end of yield plateau
$\dot{\varepsilon}_{ref}$	reference strain rate
C	Constant

4. Analysis

Finite element models of bolt and plate assembly have been developed to recreate the behaviour of threaded connections subjected for tensile load. The goal was to design setup by using FE-simulations. The sketch is shown in Fig. 10.

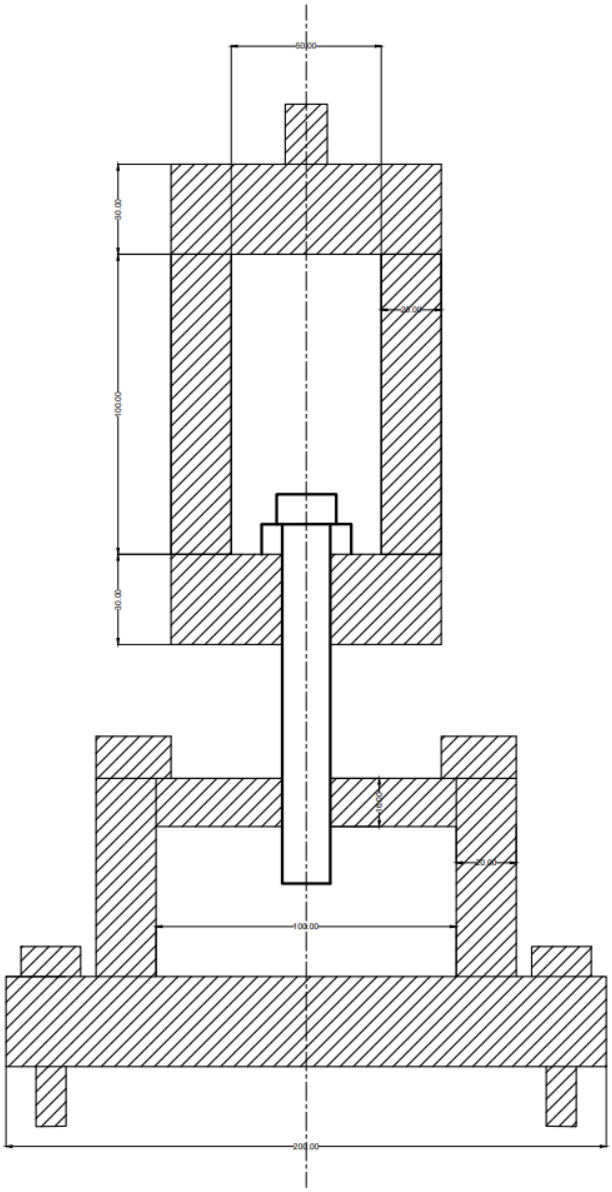

Figure 10 Illustration of laboratory test set-up

Mechanical properties of the bolt and plate material were identified from material tension tests, hardness tests and inverse modelling performed by Grimsmo (Grimsmo et al., 2016) and Skavhaug (Elin Stensrud Skavhaug, 2015) respectively:

	Bolt	Plate
σ_y [MPa]	908.7	424.0
θ_1 [MPa]	5194	7662
Q_1 [MPa]	99.70	252.1
θ_2 [MPa]	293.6	-12320
Q_2 [MPa]	3131	-83.91
ε_{p_plat} [-]	0.013	0.01

Table 1 Material properties of bolt and plate (Grimsmo et al., 2016),(Elin Stensrud Skavhaug, 2015)

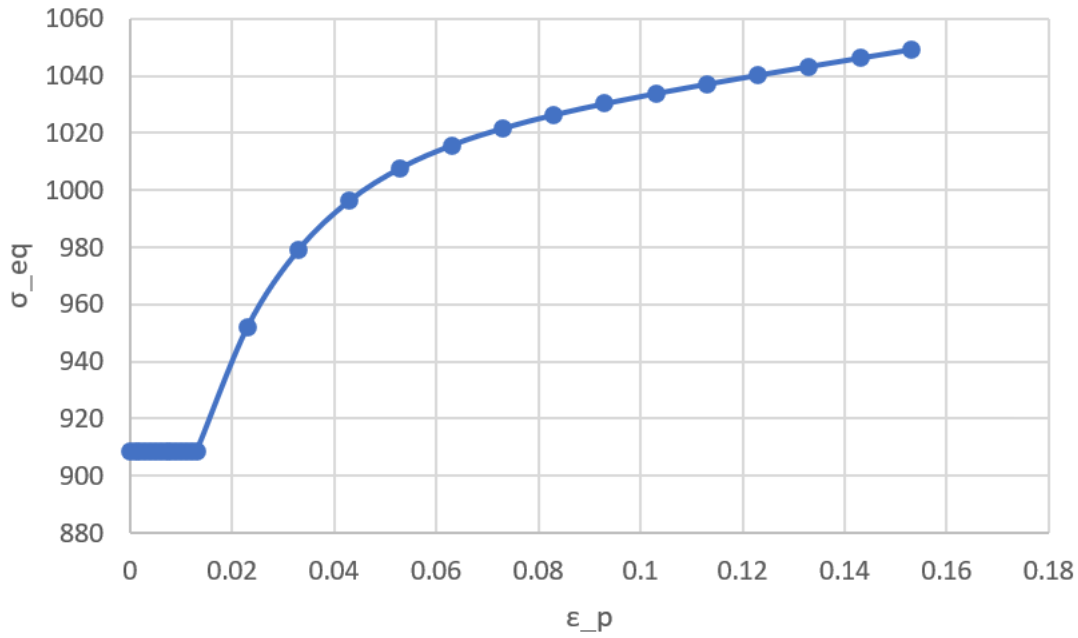

Table 2 Illustration of equivalent stress σ_{eq} versus equivalent plastic strain ε_p for bolt material

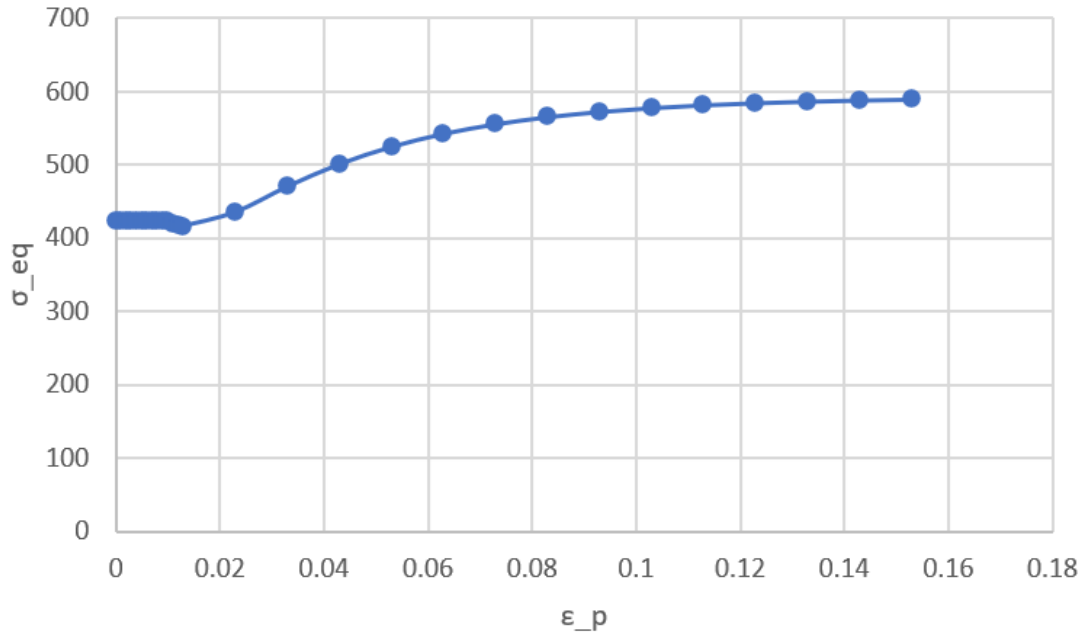

Table 3 Illustration of equivalent stress σ_{eq} versus equivalent plastic strain ε_p for plate material

4.1. Finite element analysis

An explicit integration scheme Abaqus/Explicit was used in order to utilize finite element analyses. It is prefered for the problems where the contact (also in threaded connections) is the main problem of analysis.

In the finite element models the complex helix shape of the bolt was simplified to axysimmetric two-dimensional bolt model. In the axisymmetrical model, the centerline of the bolt and the outer surface of the nut are considered to have radial symmetry.

For material parameters, two sets of inputs—linear elastic behaviour and multilinear hardening—were used due to the plasticity of metals. Materials with properties shown in Table 3 are used in FE simulation. They were assigned to elastic domain properties for bolt and plate respectively.

4.1.1. Modelling of bolt assembly

Development of the three separate models has been an integral aspect of this thesis. Every model represents different assembly configuration, i.e. bolt with a nut, bolt with a medium size plate and bolt with a big size plate.

As was mentioned above, to define multilinear behavior, two sets of input were used. Linear elastic behavior is described by the Young's modulus and Poisson's ratio and multilinear hardening is defined by the relationship between plastic strain and true stress. This first data point of multilinear hardening represents the beginning of plastic deformation.

4.1.2. Geometry

In the present study bolt M16x40 with property class 8.8 was used. Its geometry is based on ISO 68-1:1998, ISO 965-1:2013. Dimensions of the bolt and bolt threads are introduced in Appendix A. Figure 10 shows geomtry of the bolt.

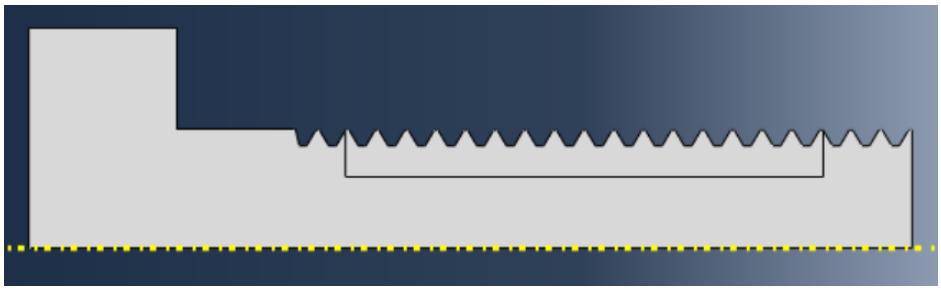

Figure 11 Geometry of the bolt M16x40

In order to study behavior of bolt in threaded holes, assembly of the bolt M16x40 8.8 and plates of three different configurations were created.

There are siplifications that were introduced in each of the three models:

- The bolt head geometry has been simplified due to the fact that the main focus of the study is the behavior of the threaded part of assembly.
- The threads were modeled as circular, ignoring their helical form.
- Due to the helical shape's neglection, several adjustments were necessary to enable the requisite grip length with the appropriate number of threads in the axisymmetric model

Model 1

Model 1 consists of the bolt M16x40 8.8 and corresponding nut. Necessary simplifications mentioned above were applied.

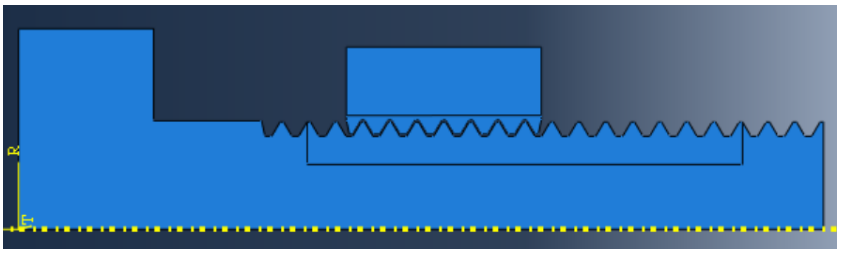

Figure 12 Geometry of the Model 1

Model 2

According to the prEN 1993-1-8, minimum thread engagement length L_t to bolt diameter d ratio for bolt property 8.8 and steel of grade S355 is 1.11. With respect to this value, model 2 consists of the bolt M16x40 8.8 and plate with diamater of 46 mm and thread engagement length of 17.6 mm.

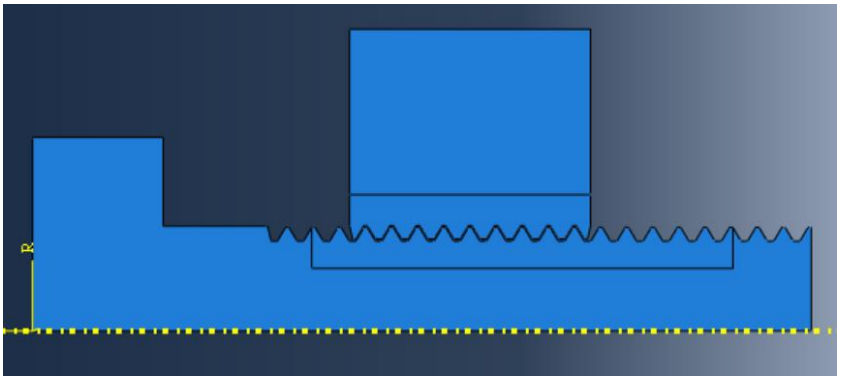

Figure 13 Geometry of the Model 2

Model 3

Model 3 consists of the bolt M16x40 8.8 and plate with diamater of 66 mm and thread engagement length L_t of 17.6 mm accorrding to the prEN 1993-1-8.

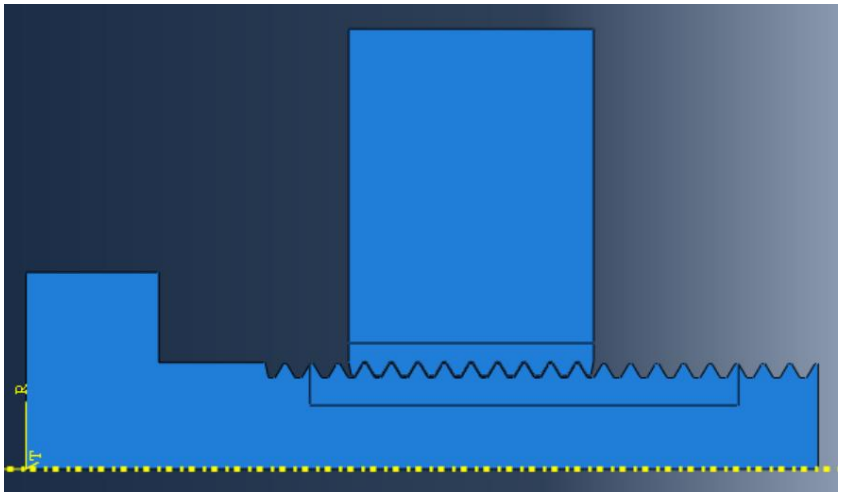

Figure 14 Geometry of the Model 3

4.1.3. Mesh characteristics

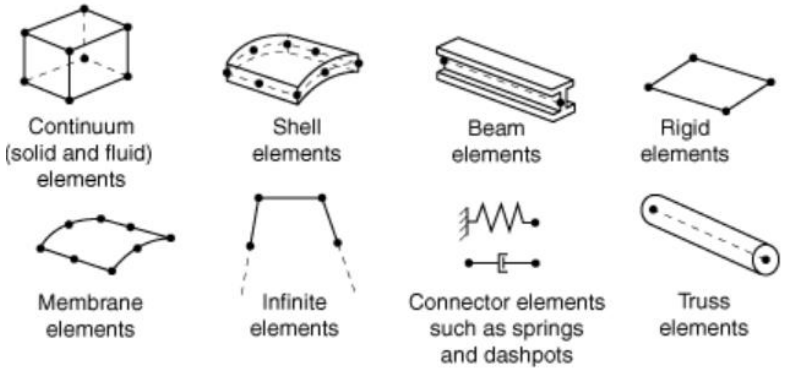

Figure 15 Illustration of element families in Abaqus (Simulia)

Because Abaqus offers such a wide range of element formulations, choosing the right finite element type is essential to getting precise and trustworthy predictions. Fig. 11 demonstrates the most used element families in stress analyses. The geometry type each family assumes is one of the key differences between various element families. Element name in Abaqus is a combination of letters and numbers, where the first letter of an element's name designate its family. Number states for the quantity of nodes in the element and R in the end of the name indicates reduced integration (Simulia).

In the present models of bolt and plates a 4-node bilinear axisymmetric quadrilateral, reduced integration, element CAX4R is used. Reduced integration decreases computational time. However, hourglassing frequently occurs with reduced-integration parts. If only one integration point is employed, then as shown in Fig. 12 the element's x-direction (green arrow) and y-direction (red arrow) remain unchanged while bending. Thus the element cannot "understand" bending. Elements often become overly flexible as a result of a numerical miscalculation. As element size grows, this issue gets more evident since each element must represent more bending. Hence, the overpredicted deflection might occur.

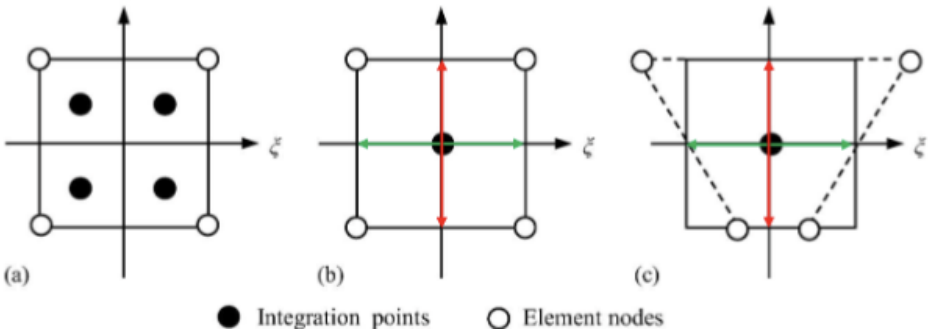

Figure 16 Illustration of hourglassing effect (Grytten, 2021)

In order to obtain more accurate results and lessen the possibility of hourglassing effect, bolt and plate in each of three models were partitioned. Thus finere mesh in areas where the contact between threads occurs was given (Fig.11).

Type of mesh	Element size for the bolt mesh (CEN)		Element size for the plate mesh (CEN)	
	Local mesh (mm)	Global mesh (mm)	Local mesh (mm)	Global mesh (mm)
Coarse	0.5	1	0.5	1
Medium	0.4	1	0.4	1
Fine	0.3	1	0.3	1

Table 4 Distribution of different element sizes

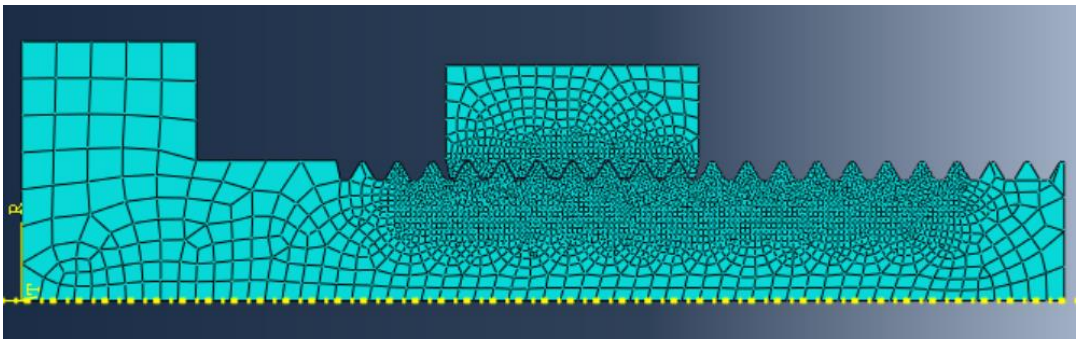

Figure 17 Illustration of mesh distribution

4.1.4. Boundary conditions

Finite element models incorporate axisymmetric boundary conditions to simulate laboratory test scenarios. Triangles and arrows in the fig.14 represent fixed boundary condition and force respectively. The longitudinal movement of the steel plate was constrained. It was created to stop the plate from shifting in a vertical direction. At the base of the bolt head, the velocity boundary condition was added.

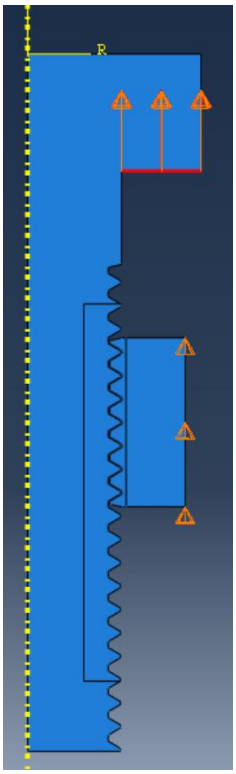

Figure 18 Illustration of boundary conditions

4.1.5.Interactions

Surface-to-surface contact was used between bolt threads to nut/plate threads. For this type of contact, there are two important aspects, i.e., tangentianal behavior and normal behavior. For tangential behavior, isotropic Penalty model was used. In each of three models friction coefficient μ=0.2 was used. It correspond to the value for the rolled surfaces indicated in NS-EN 1090-2. For the normal behavior "Hard" contact was chosen.

4.1.6.Computational efficiency

One of the tools for increasing computing efficiency that has already been stated is reducing the number of elements. Mass scaling is another tool frequently utilized in ABAQUS/Explicit. It is frequently helpful to shorten the analysis's runtime or artificially increase the model's mass (a process known as "mass scaling") in order to obtain an effective solution. If model is rate dependent, mass scaling is the favored method of shortening the solution time since the natural time scale is kept. However, both options produce comparable results for rate-independent materials. Within the quasi-static analysis it is typical to scale the entire model. As a result, it is never required to lower a model's mass below its physical value, and it is typically not viable to raise mass arbitrarily without sacrificing accuracy. The majority of quasi-static scenarios typically allow for a little amount of mass scaling, which will raise the time increment used by ABAQUS/Explicit and decrease processing time. However, care must be taken to avoid drastically changing the solution due to changes in the mass and ensuing increases in inertial forces. (Simulia)

In the present study semi-automatic mass scaling was used. Chossen type was applied to the whole model. Target time increment t_{cr} was set to 0.001 s. When employing the semi-automatic mass scaling, elements are scaled with various factors so that every element reaches the critical mass. The smallest components found in the threaded portion of the bolt and nut will thereafter be scaled by the highest factor, resulting in the largest mass.

5. Parameter study with respect to plate size

5.1. Mesh sensitivity

Coarse mesh can be used for solving problems, but sometimes coarse mesh lead to the inaccurate result. In the same time using of fine mesh can significantly increase computational cost. Therefore appropriate mesh size that will have a less computational cost and in the same time will give an accurate result should be chosen. For this purpose mesh sensitivity study was performed.

In a mesh sensitivity research, the same simulation is performed with grids of varying resolutions, and the amount that the converged solution varies with each mesh is examined.

Table 4 describes element sizes that were used for study. Force- displacement curves, shown in Fig. 18-20 indicates minimal discrepancies of the graphs with element size of 0.5 mm or less. It means that asymptotic convergence zone is reached. Hence, in each of three models mesh with element size of 0.5 mm or less is appropriate for further analysis.

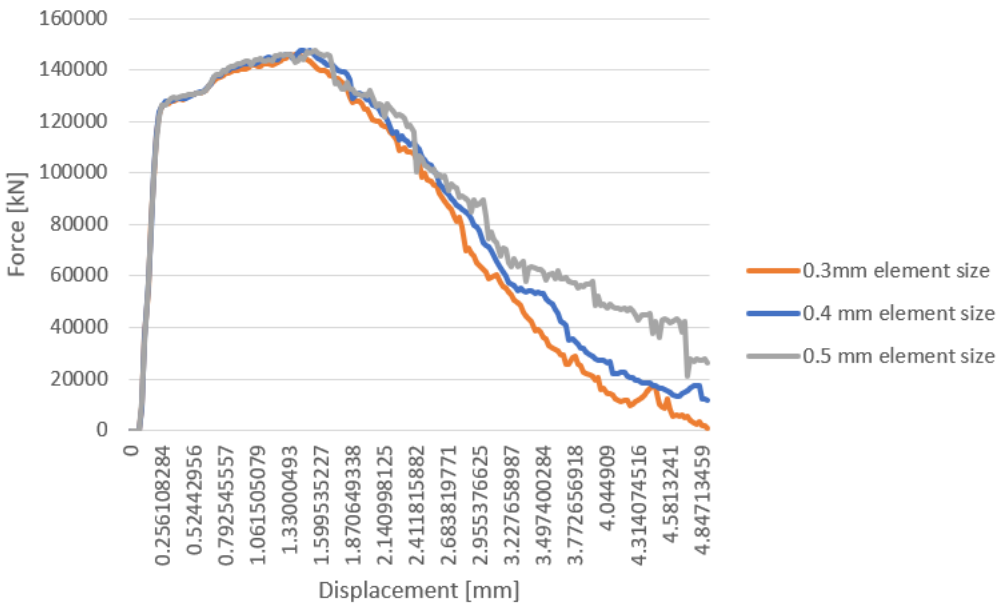

Figure 19 Force- displacement curve for Model 1

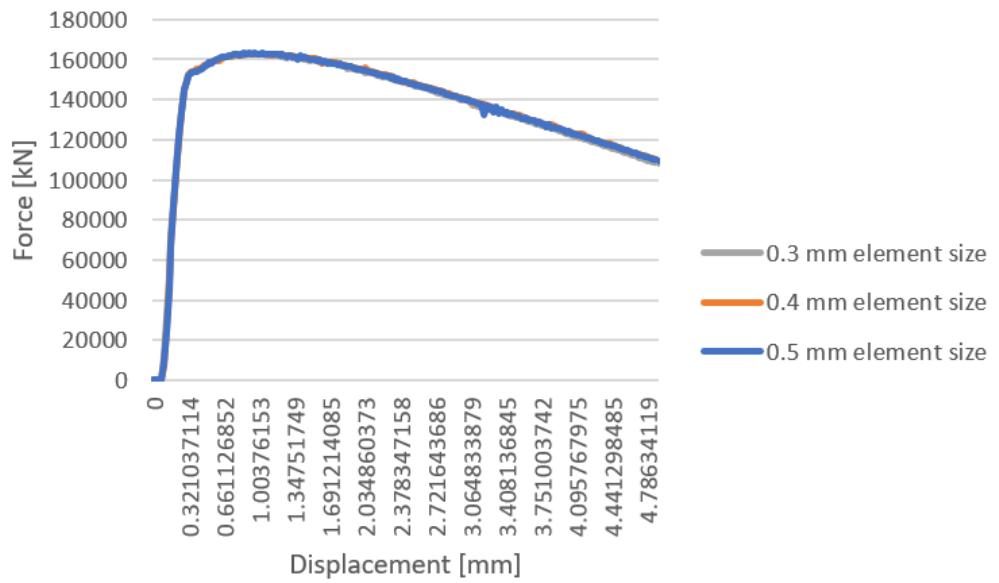

Figure 20 Force- displacement curve for Model 2

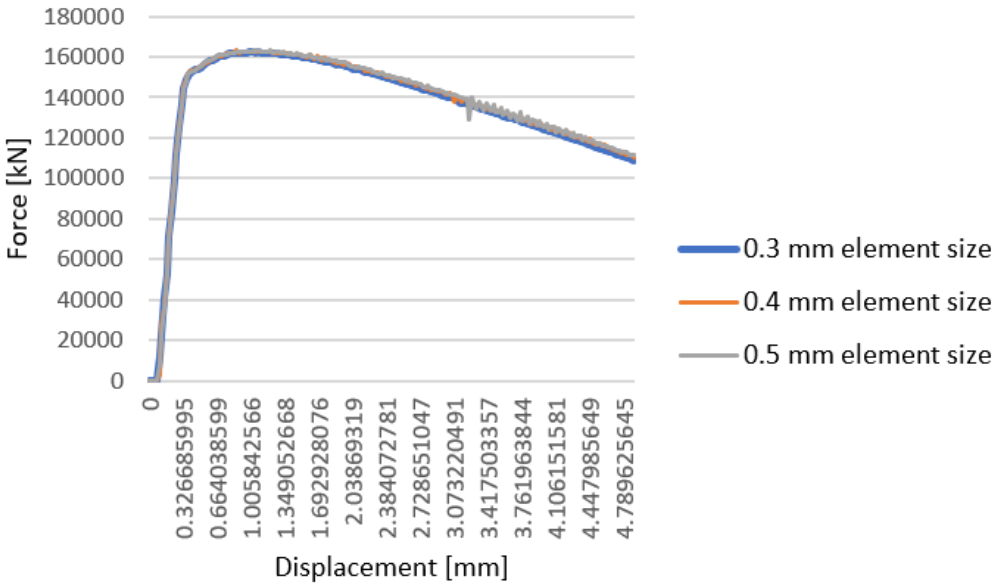

Figure 21 Force- displacement curve for Model 3

5.2. Geometry of the plate

Simulations of direct tension tests was performed on three models. Each of them consists of the bolt M16x40 8.8 and plate of different geomtery as was mentioned in preivous chapters. According to Grimsmo (Grimsmo et al., 2016), bolt fracture, bolt thread failure, and nut thread failure are the three most frequent failure types of tension-loaded bolt and nut assemblies. The last two failure scenarios are both referred to as thread failures.

Model 1consists of the bolt and a nut of appropriate size. Nut in Model 1 represents plate of the smallest size from all three models. Stress fields, shown in fig. 21-23 indicate that this model is subjected to thread failure.

Models 2 and 3 consist of the bolt and a plate with diameter 46 mm and 66 mm respectively. Illustrations of stress fields of Model 2 and Model 3 (Fig. 24-29) demonstrate that in contrast with Model 1, models 2 and 3 are subjected to a bolt fracture. It reveals that larger size of the plate leads to a signinficant difference in a model behavior. Hence use of the smaller plate can lead to a thread failure that is according Grimsmo (Grimsmo et al., 2016) is typically undesirable because this failure mode is less ductile than bolt fracture mode.

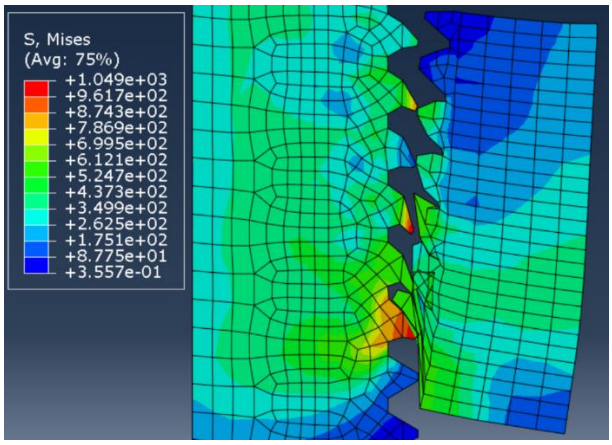

Figure 22 Deformation of Model 1 (element size 0.5mm)

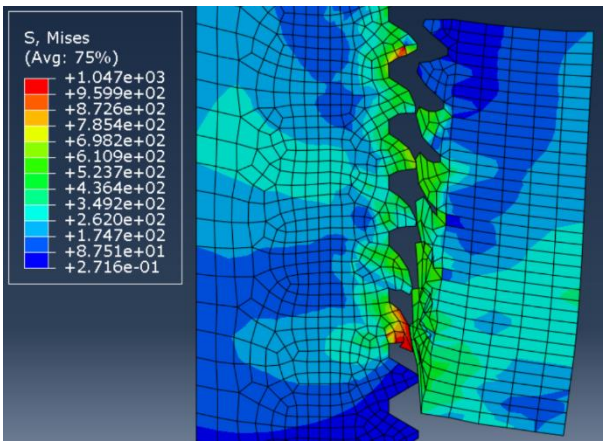

Figure 23 Deformation of Model 1 (element size 0.4mm)

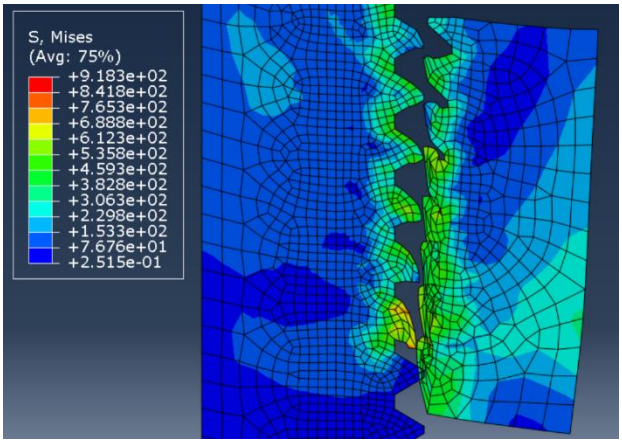

Figure 24 Deformation of Model 1 (element size 0.3mm)

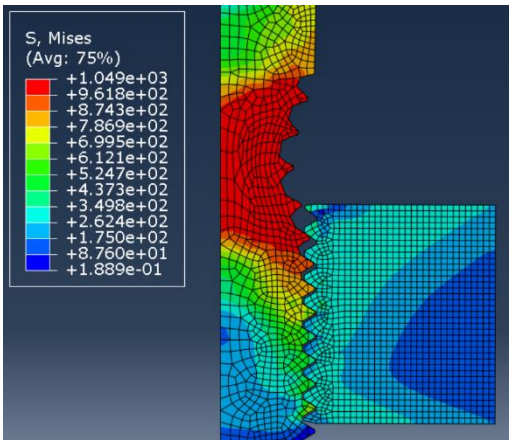

Figure 25 Deformation of Model 2 (element size 0.5mm)

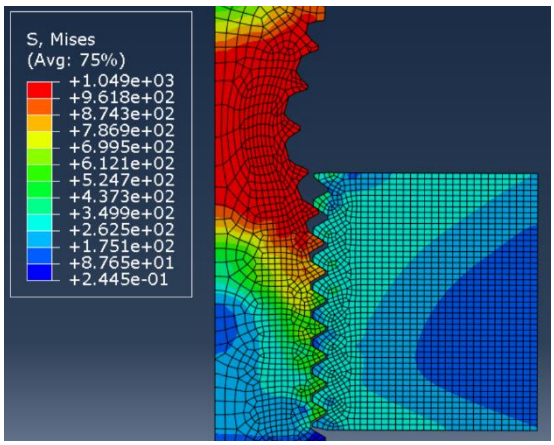

Figure 26 Deformation of Model 2 (element size 0.4mm)

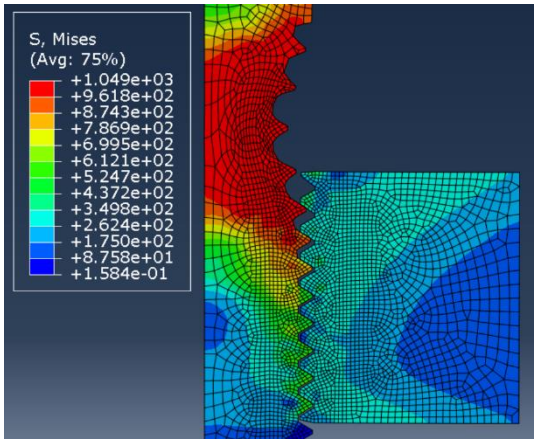

Figure 27 Deformation of Model 2 (element size 0.3mm)

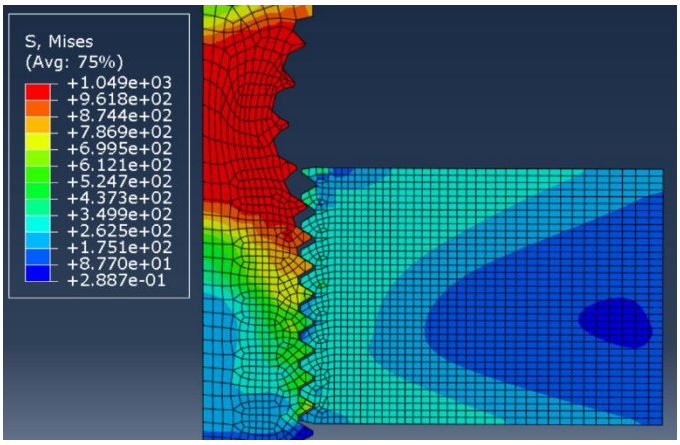

Figure 28 Deformation of Model 3 (element size 0.5mm)

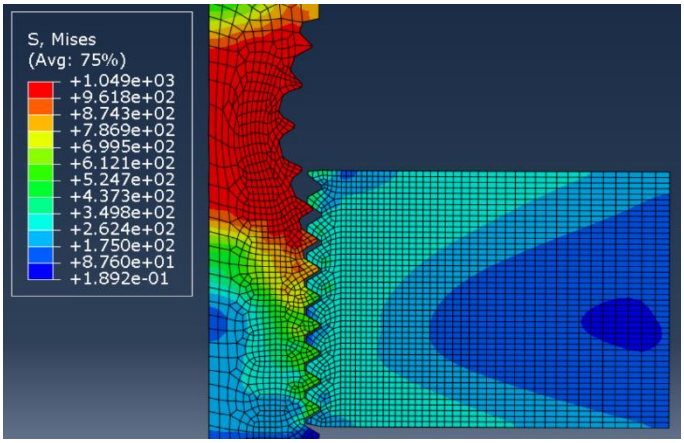

Figure 29 Deformation of Model 3 (element size 0.4mm)

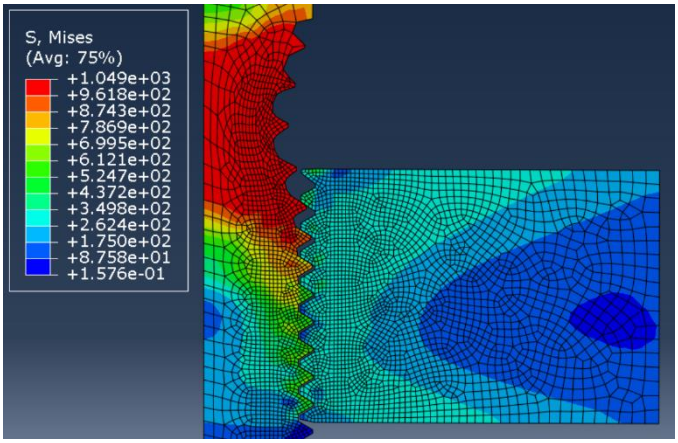

Figure 30 Deformation of Model 3 (element size 0.3mm)

6. Discussion

6.1. Multilinear plasticity hardening model

In the present study multilinear hardening model was used. A multilinear hardening model uses a piece-wise linear function to model nonlinear strain hardening response until the necking begins. Multilinear model can only capture the response up to onset of necking and does not support the portion of the curve with negative slope. There are other material models that can capture the damage in the material. for example Johnson-Cook material model that is described in Appendix B.

6.2. Thread failure

For the threaded joints in tension there are two types of failure most common: bolt shank breakage and thread failure. As can be seen in a stress field of the model 1 (Fig. 22-24), assembly with the smallest plate size is exposed to the thread failire type.

The greatest stress values model shows in the area of the first few threads. Of all the engaged threads, the first thread usually carries the most weight. The stress concentration in the thread root is maximum at this thread since there is just one nearby load-bearing thread.

M. J. O'Brien and R. G. Metcalfe (2009) mean, that by including at least two full fastener threads (up to one diameter) above and below the nut, the stress concentration at the initial few threads will be diminished.

6.3. Bolt shank breakage

As was indicated above, another common type of failure of threaded joints is bolt shank breakage. In the present study plates in model 2 and 3 has a larger thickness, compared to model 1. Hence the threaded length L_t is increase.

Stress fields of the models 2 and 3 presented in Fig.25-30 show that these models are subjected to the boolt shank breakage. Therefore it is possible to assume that as the threaded length L_t increases, a change from thread failure to bolt fracture can be seen.

Grimsmo (2016) has revealed that placing of the nut also affects failure mode of assembly. He means that placing the nut close to the thread run-out, i.e. near the unthreaded portion of the bolt (the shank), led to thread failure, whereas placing the nut sufficiently far from the thread run-out led to bolt fracture.

6.4. Parameters of the plate

Models 2 and 3 consist of the same bolt type and plates of the same thickness. The difference lies in the diameter value of the plate. As was mentioned above, diameter of plate in model 2 is 46 mm and diameter of plate in model 3 is 66 mm.

Force-displacement curves (Fig. 20-21) for both models are almost identical. Hence it is possible to assume that diameter difference in 20 mm was insufficient to draw a conclusion about the nature of the change in forces when changing the diameter of the plate.

Thus, additional tests may be an option for further study of this topic. It is possible to explore combinations of various geometries. For example, using a larger diameter bolt while maintaining the plate parameters.

7. Conclusion

The dimensions of the bolt and the plate, the material qualities of the bolt and the plate, and the loading technique all affect the tensile resistance of bolts in threaded holes. Due to the threaded connection, a bolt that is subjected to tensile force receives both shear stress and direct tensile stress. The following factors therefore have significant impact onto bolt's tensile resistance:

- Materials for bolts and plates: A key consideration is the tensile strength of the bolt and plate materials. Bolts and plates are frequently composed of materials like steel or stainless steel, each with varying strengths.
- Bolt diameter: The bolt's diameter directly affects its tensile resistance. In general, a larger-diameter bolt manufactured of the same material may bear greater tensile loads than a smaller-diameter bolt.
- Structural Strength: Steel plates that are thicker generally have a larger ability to carry loads and are more force-resistant.
- Engagement of the threads: The strength of the connection is influenced by the engagement length of the threads in the hole. The load-bearing surface and overall strength of the threaded joint are increased by a longer engagement length.
- Thread pitch: The tensile resistance is also influenced by the thread pitch. Greater resistance to tensile forces is achieved by using finer threads since they distribute the load over more threads and provide a bigger load-bearing surface.
- Thread fit: The alignment of the bolt and the threaded hole affects how loads are distributed and how strong the joint is. For instance, compared to a tighter interference fit, a clearance fit may make assembly easier but may have lower load-carrying capacity.

Bibliography

Alexander, E. M. (1977). Analysis and Design of Threaded Assemblies. *SAE Transactions*, *86*, 1838-1852. http://www.jstor.org/stable/44644510

CEN. (2023). FprEN 1993-1-8:2023. In.

Elin Stensrud Skavhaug, S. I. Ø. (2015). *Tension-loaded bolted connections in steel structures* NTNU]. Trondheim.

Grimsmo, E. L., Aalberg, A., Langseth, M., & Clausen, A. H. (2016). Failure modes of bolt and nut assemblies under tensile loading. *Journal of Constructional Steel Research*, *126*, 15-25. https://doi.org/https://doi.org/10.1016/j.jcsr.2016.06.023

Grimsmo, E. L., Aalberg, A., Langseth, M., & Clausen, A. H. (2017). How placement of nut determines failure mode of bolt-and-nut assemblies [Article]. *Steel Construction*, *10*(3), 241-247. https://doi.org/10.1002/stco.201710025

Grytten, F. (2021). *Notes from the course/MABY 4100/* [University lectures].

He, A., Xie, G., Zhang, H., & Wang, X. (2013). A comparative study on Johnson–Cook, modified Johnson–Cook and Arrhenius-type constitutive models to predict the high temperature flow stress in 20CrMo alloy steel. *Materials & Design (1980-2015)*, *52*, 677-685. https://doi.org/https://doi.org/10.1016/j.matdes.2013.06.010

Huang, A. K. S. (1995). *«Continuum Theory of Plasticity»*. John Wiley & Sons Inc.

Kumar Reddy Sirigiri, V., Yadav Gudiga, V., Shankar Gattu, U., Suneesh, G., & Mohan Buddaraju, K. (2022). A review on Johnson Cook material model. *Materials Today: Proceedings*, *62*, 3450-3456. https://doi.org/https://doi.org/10.1016/j.matpr.2022.04.279

Lin, Y. C., Chen, X.-M., & Liu, G. (2010). A modified Johnson–Cook model for tensile behaviors of typical high-strength alloy steel. *Materials Science and Engineering: A*, *527*(26), 6980-6986. https://doi.org/https://doi.org/10.1016/j.msea.2010.07.061

Nord-Lock, G. (2023). *THE HISTORY OF THE BOLT*. https://www.nord-lock.com/insights/knowledge/2017/the-history-of-the-bolt/#:~:text=What%20were%20bolts%20originally%20used,use%20for%20around%20400%20years. Accessed: 2023-03-10

O'Brien, M. J., & Metcalfe, R. G. (2009). High Strength Engineering Fasteners: Design for Fatigue Resistance. *Journal of Failure Analysis and Prevention*, *9*(2), 171-181. https://doi.org/10.1007/s11668-009-9213-6

Reyes, A. (2022). *Notes from the course/MABY 4400/*

Simulia. *Abaqus Analysis User's Manual* http://130.149.89.49:2080/v6.10/books/usb/default.htm?startat=pt06ch24s01abo23.html Accessed: 2023-05-01

Wang, L., & Tong, W. (2015). Identification of post-necking strain hardening behavior of thin sheet metals from image-based surface strain data in uniaxial tension tests. *International Journal of Solids and Structures*, *75-76*, 12-31. https://doi.org/https://doi.org/10.1016/j.ijsolstr.2015.04.038

Appendices

Appendix A

Geometry of the bolt

This appendix includes pictures and geometrical measurements of bolts and nuts with accordance to the relevant standards.

Bolt marking consists of a set of letters and numbers indicating certain properties. All general metric threads begin with M to indicate that they are metric. A number that denotes the external thread major diameter follows it. Last number refers to the pitch. There may be an additional designation following the pitch in case of tolerances.

For the external thread (Fig.32), any tolerance is based on the size reduction, as it cannot be larger than the fundamental or standard profile. In any other case, it will obstruct the nut's internal thread. Thus, small letters (d, d_1, d_2) represent negative tolerance of external thread.

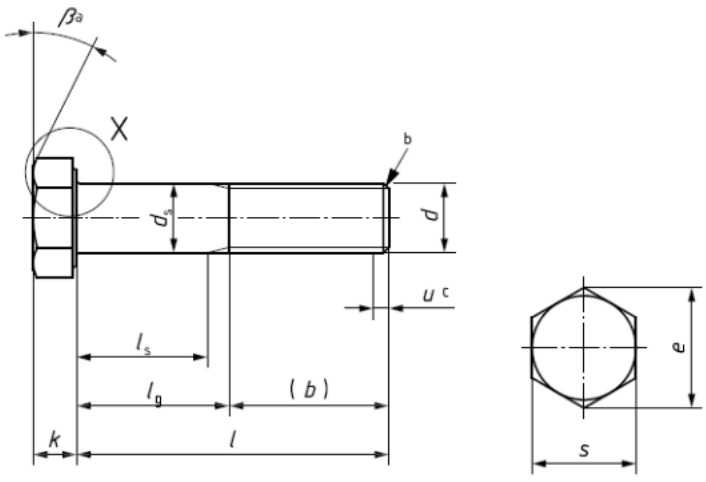

Figure 31 Geometry of threaded bolt and bolt head according to NS-EN 14399-3:2015

Internal thread, opposite, has a positive tolerance. It explained by the fact, that the internal thread of the nut cannot be any smaller than the standard profile and must result in an increase in size. Hence, capital letters (D, D_1, D_2), represent positive tolerance of internal thread.

A common major, minor, and pitch diameter are shared by the threads of the nut and screw. The major and pitch diameters are the main factors in the screw thread. Both d_1 and d_2 are used to refer to it. The nut, however, concentrates on the minor and pitch diameters. They are shown as D_1, and D_2 (Fig.32)

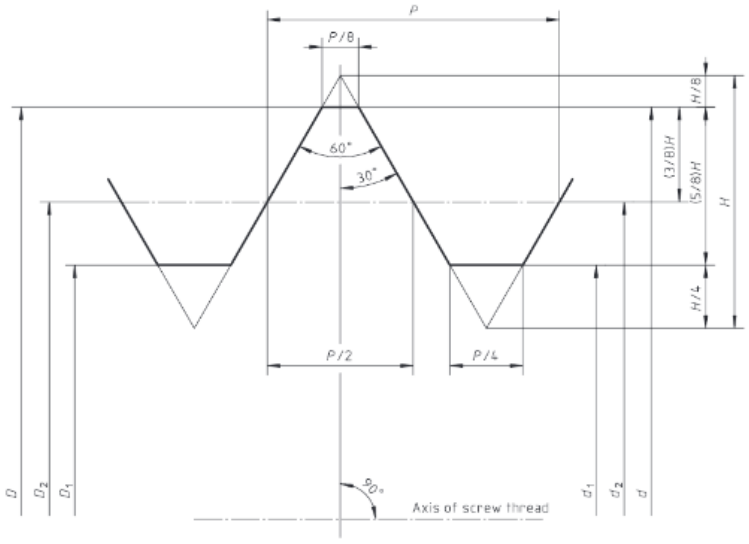

Figure 32 Geometry of threads. ISO 68-1

For the present study bolt M16 with a length of 40 mm was used. Its geometry (Fig. 33) was developed according to the NS-EN 14399-3:2015, ISO 724:1993, ISO 68-1:1998, ISO 965-1:2013.

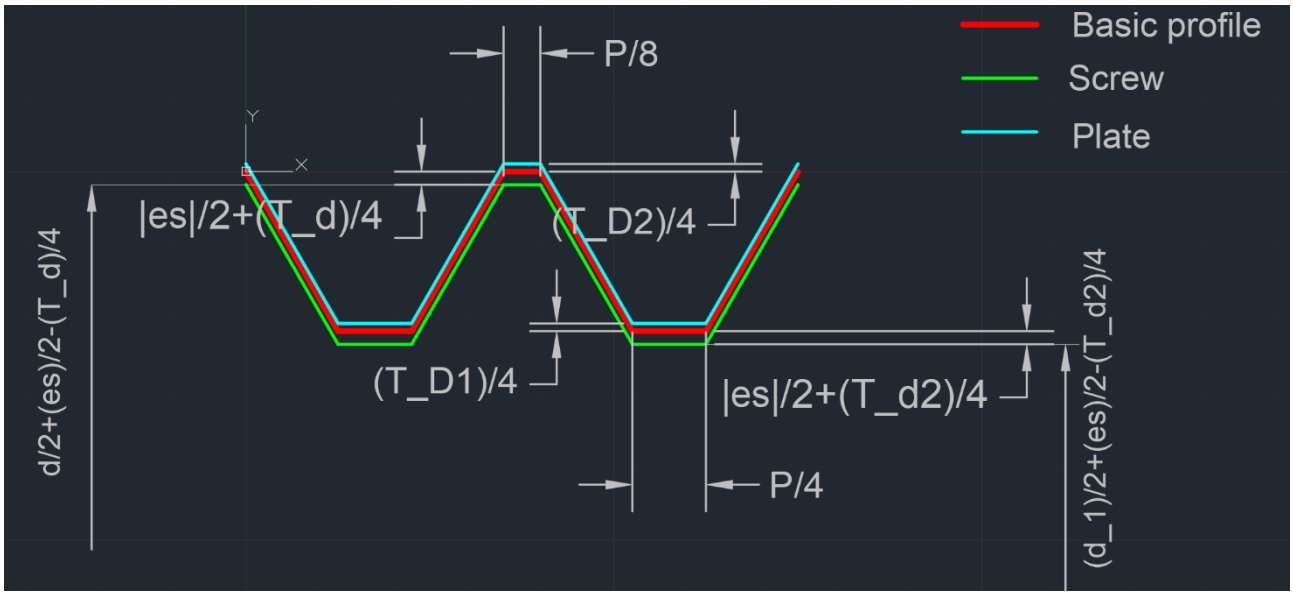

Figure 33 Geometry of threads with adjustments according to ISO 965-1:2013

Appendix B

Johnson Cook model

A consistent and accurate depiction of material behavior, where strain, strain rate, and temperature have an impact on the material flow stress, is required for the design and optimization of process parameters in the metal forming sector.

Johnson and Cook first proposed the Johnson-Cook model in 1983. This model is suitable for expressing the relationships between stress and strain in metallic materials under situations of significant deformation, rapid strain rate, and high temperature. It has been widely used since it was first proposed because of the straightforward form. (He et al., 2013). The initial Johnson-Cook model (Lin et al., 2010) can be written as follows :

$$\sigma = (A + B * \varepsilon^{n})\,(1 + C * ln\,\dot{\varepsilon}^{*})\,(1 - T^{*m})$$

A - yield stress of the material under reference conditions

B - strain hardening constant

$\dot{\varepsilon}$ - strain

n - strain hardening coefficient

C - strengthening coefficient of the strain rate

ε^{*} - strain rate

T^{*m} - temperature

m - thermal softening coefficient

Three parentheses are included in the equation show strain hardening effect, strain rate strengthening effect and temperature effect, that influences the values of flow stress. These effects are listed from left to right (Kumar Reddy Sirigiri et al., 2022).

In the Johnson-Cook model's expression (Lin et al., 2010):

$$\dot{\varepsilon}^{*}=\frac{\dot{\varepsilon}}{\dot{\varepsilon}_{0}}$$

$\dot{\varepsilon}^{*}$ - dimensionless strain rate

$\dot{\varepsilon}$ - strain rate

$\dot{\varepsilon}_{0}$ - the reference strain rate

$$T^{*}=\frac{T-T_{r}}{T_{m}-T_{r}}$$

T^{*}- homologous temperature

T_{m}- melting temperature

T - absolute temperature

T_{r} - reference temperature